Bulletin of the Seismological Society of America, Vol. 76, No. 6, pp. 1623–1640, December 1986

RUPTURE PROCESS OF THE 1983 JAPAN SEA (AKITA-OKI) EARTHQUAKE USING A WAVEFORM INVERSION METHOD

BY EIICHI FUKUYAMA AND KOJIRO IRIKURA

ABSTRACT

The rupture process of the 1983 Japan Sea earthquake (M_{JMA} = 7.7) is determined by applying waveform inversion of displacement-type, strong motion records based on the Bayesian method. The synthesis of the seismic motions from the main shock is made using the records from the two aftershocks (M_{JMA} = 7.1 and M_{JMA} = 6.1) as empirical Green's functions. The main shock fault consists of two subfaults. The aftershock (M = 6.1) occurring south of the main shock fault is used for the southern subfault empirical Green's function and the aftershock (M = 7.1) occurring north of the main shock fault is used for the northern subfault. In this synthesis, it is not necessary to calculate propagation path and local site effects. Therefore, the information about the source process can be extracted from the comparison between observed seismic motions and the synthetic ones without detailed information on the velocity structure along the whole path from the source to each station. The inversion for the rupture process is attempted for both a line source model and an area source model. In both models, the main shock fault surface is divided into several elements whose sizes are determined from the scaling relations between the main shock and its aftershocks. The slip displacement and the rupture starting time on each element are estimated as model parameters in the inversion. A good convergence is obtained after about 10 iteration steps for the line source case and after 5 iteration steps for the area source case. The results are summarized: (1) the average rupture velocity is approximately 2.5 km/sec for the southern subfault and 2.0 km/sec for the northern subfault, and (2) there is a large slip displacement near the rupture initiation point and the north edge of the fault. Thus, there is considerable heterogeneity in rupture propagation and slip distribution over the fault plane.

INTRODUCTION

High quality records of strong ground motions and detailed studies of synthetic seismograms have demonstrated that fault rupture during large earthquakes is nonuniform both in space and time. The heterogeneity of the fault rupture process has important consequences not only for the nature of the earthquake source but also for the prediction of strong ground motions during large earthquakes. The purpose of this paper is to show how the irregularity of fault motions can be derived by inverting near-field seismic records.

Heaton and Helmberger (1979), who determined the slip distribution over the fault surface of the 1971 San Fernando earthquake, demonstrated the heterogeneity of the fault slip by comparing synthetic seismograms based on the Cagniard-de Hoop solution with the strong ground motions observed during the earthquake by the forward modeling. Since then, several authors have applied inversion techniques to estimate the fault heterogeneity or fault motion complexity. The techniques employed in these studies include three different types. The first one consists of determining the dislocation at each grid point of a finely segmented net that covers the fault, by the point-by-point inversion method (e.g., Hartzell and Heaton, 1983). The second consists of calculating moment rate functions at several stations

surrounding the source area using a deconvolution method to determine where the large moment was released on the fault plane (e.g., Kikuchi and Kanamori, 1982; Ruff and Kanamori, 1983). The third consists of determining the nonuniformness of dislocation and rupture propagation over the fault directly by using the isochron method (e.g., Spudich and Frazer, 1984).

To examine the source process, we need to separate the source effect from the others, such as local site and path effects. All of these techniques discussed above require some knowledge of the geological structure along the propagation path to each recording station. Recently, a method for synthesizing seismograms from larger events has been successfully developed using the seismograms of smaller events as empirical Green's functions (Hartzell, 1978; Kanamori, 1979; Hadley and Helmberger, 1980; Irikura and Muramatsu, 1982). This method has the advantage that we need not remove the propagation effects. Then, we propose this fourth method to extract the inhomogeneity of the source process. First, we calculate synthetic seismograms for a main shock using aftershock records as empirical Green's functions. Second, we calculate the cross-correlation error functions between observed and synthesized seismograms. Third, by applying the Bayesian method for a nonlinear inversion problem, we obtain the rupture propagation and slip distribution over the fault, which minimize the cross-correlation error functions. Some of the advantages of this method are: (1) we need not take into account the path effects; (2) we need not know the absolute time in each seismogram; and (3) we can directly combine *a priori* information as initial values to the inversion procedure. The features of (1) and (2) increase the amount of seismic data available for inverting for the source process.

We applied this method to the 1983 Japan Sea (Akita-Oki) earthquake. This event occurred on 26 May 1983 in the Japan Sea off the western coast of northern Honshu [Japan Meteorological Agency (JMA), 1984]. The JMA network recorded strong motions with low-gain displacement seismographs of both the main shock and the two largest aftershocks at stations located at distances between 150 and 300 km away from the epicenter surrounding the source region in a semi-circle. In this paper, we have applied the new method discussed above to quantify the irregularities of the rupture process on the fault by inverting these data. We also discuss the resolution and reliability of the above method.

Synthetic Seismograms Using Empirical Green's Functions

To calculate synthetic seismograms using aftershock records as empirical Green's functions, we follow the method by Irikura (1983). First, we assume the similarity relation between large and small earthquakes (Aki, 1967). From the similarity relation, we can derive the formula below (Kanamori and Anderson, 1975; Geller, 1976).

$$L/L_e = W/W_e = D/D_e = t/t_e = (M_0/M_{0e})^{1/3} \tag{1}$$

where L and W are the length and width of the fault, D is the final offset of the slip displacement, t is the rise time, M_0 is the seismic moment, and the parameters with subscript "e" are for the small event used as an empirical Green's function. (Those without subscript "e" are for the large events to be synthesized.) We divide the fault surface into several elements. When assuming a line source model, we divide the fault surface into N elements, and when assuming an area source model, we divide

the fault surface into $N \times N$ elements where N is determined by

$$N = (M_0/M_{0e})^{1/3}. \tag{2}$$

We calculate synthetic seismograms by the equation (3) derived by Irikura (1983), which gives the ground motion at the observation station as

$$\boldsymbol{U}(\boldsymbol{x}, t) = \sum_{i=1}^{N} \sum_{k=1}^{N} R_i/R_e \cdot (r_e/r_i)^p \, m_i \cdot N \cdot \boldsymbol{U}_e(\boldsymbol{x}, t - t_{ik}^*) \tag{3}$$

for the line source model, and

$$\boldsymbol{U}(\boldsymbol{x}, t) = \sum_{i=1}^{N^2} \sum_{k=1}^{N} R_i/R_e \cdot (r_e/r_i)^p \, m_i \cdot \boldsymbol{U}_e(\boldsymbol{x}, t - t_{ik}^*)$$

for the area source model, where

$$t_{ik}^* = (r_i - r_e)/v_c + t_{ik} \tag{4}$$

and R_i is the radiation pattern, r_i is the focal distance for the ith element, and v_c is the phase velocity of the wave of interest. p is 1 for the body waves and $\frac{1}{2}$ for the surface waves. The usage of subscript "e" in equations (3) and (4) is for the small event as in equation (1). Here, we assume that

$$t_{ik} = t_i + (k - 1)t_e \tag{5}$$

where t_i is the starting time of the rupture at ith element, and t_e is the rise time of the small event. A schematic illustration for the synthesis is shown in Figure 1.

We introduce a new parameter m_i which is not defined in Irikura (1983). If the scaling relation (1) holds exactly at all elements of the fault, m_i should be unity. However, in reality, the scaling relation is considered to give the average information about the fault, and so there must be some local stress release fluctuations around

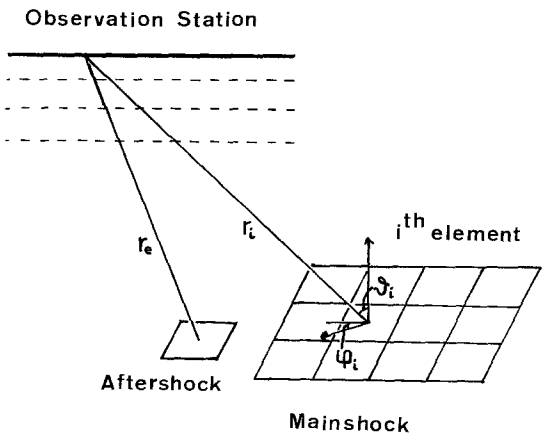

FIG. 1. Schematic model which shows the relation between the aftershock and the ith element of the main shock.

the average. Now, for the sake of simplification, we here assume the rise time is constant at each element. Therefore, the fluctuations affect only the parameter m_i, i.e., m_i stands for the inhomogeneity over the fault. We estimate parameters m_i and t_i in the inversion procedure to be introduced in the next section.

Inversion Procedure

The parameters to be estimated by inverting observed data are m_i and t_i in equation (3). Although parameter m_i can be linearly linked to the synthetic seismograms, parameter t_i cannot be, and then we need to use a nonlinear inversion technique. We use here the cross-correlation error function proposed by Mellman (1980) as the data used in the inversion procedure. This approach has the advantage that we can use the information from the seismic time series even if we do not accurately know the arrival times of the seismic waves. The cross-correlation error function y_i for the ith station is

$$y_i = 1 - \int O_i(t) S_i(t + t_{\max})\, dt \Big/ \left(\left[\int O_i(t)^2\, dt \right]^{1/2} \left[\int S_i(t)^2\, dt \right]^{1/2} \right) \tag{6}$$

where $O_i(t)$ is the observed seismogram for the ith station, and $S_i(t)$ is the synthesized seismogram. $t_{\max}$ is the lag time which minimizes y_i. According to the Bayesian approach (Jackson and Matsu'ura, 1985), we can easily find the solution by the implicit equation

$$A^T E^{-1} e + D^{-1} d = 0 \tag{7}$$

where A, e, d, E, and D are defined in equations (A11), (A4), (A5), (A6), and (A7) in the Appendix, respectively. We outline the derivation of equation (7) in the Appendix (see also Jackson and Matsu'ura, 1985).

We solve the nonlinear problem (7) using the Gauss-Newton algorithm derived by Tarantola and Valette (1982). The $(k + 1)$th solution x_{k+1} can be obtained by

$$x_{k+1} = x_k + b M_k^{-1} r_k \tag{8}$$

$$M_k = A_k^T E^{-1} A_k + D^{-1} \tag{9}$$

$$r_k = A_k^T E^{-1} e_k + D^{-1} d_k \tag{10}$$

where b is a constant between 0 and 1. We also consider the partitioned resolution matrices to separate the estimators operating on *a priori* information and observational data from each other (Jackson, 1979). These resolution matrices (HA for observational data and KI for *a priori* data) are defined as

$$\begin{aligned} H &= M^{-1} A^T E^{-1} \\ K &= M^{-1} D^{-1} \\ M &= A^T E^{-1} A + D^{-1} \end{aligned} \tag{11}$$

and

$$I = HA + KI \tag{12}$$

where I is the unit matrix. $(HA)_{tr}$ and $(KI)_{tr}$ are the traces (sum of the diagonal elements) of HA and KI, respectively, and the ratio $(HA)_{tr}/(KI)_{tr}$ indicates how much information we have derived from the observed data.

The algorithm we use here to find the solution of equation (7) consists of two steps. *Step 1*: we estimate the parameters through equations (8), (9), and (10). The convergence criterion of step 1 is that r_k of equation (10) is either equal or very close to zero. *Step 2*: we calculate $(HA)_{tr}/(KI)_{tr}$ and compare this ratio with the convergence criterion (we adopt 0.1 for the present analysis for the line source model) of step 2. If the ratio is greater than the criterion, we change the initial parameters for the final parameters of step 1, and then we perform step 1 algorithm repeatedly until $(HA)_{tr}/(KI)_{tr}$ is less than the criterion.

DATA

We synthesize the ground motions from the main shock of the 1983 Japan Sea earthquake using the records from the two largest aftershocks (M = 7.1 and M = 6.1) and compare the synthetic seismograms with the observed seismograms from the main shock. The locations of the JMA network stations we use in this analysis and the aftershock distribution are shown in Figure 2. The epicenters of the main shock and the two aftershocks are shown as solid circles, and their focal mechanisms are also shown to the left. The epicentral distances to these stations range from 150 to 300 km, and the stations are distributed encircling the source area with the coverage angle of approximately 190°.

We use the two horizontal component records (NS and EW) with JMA-type displacement strong motion seismographs. At each station, two types of the strong motion seismographs with different magnification are installed, i.e., one has unity magnification (S-type) and the other, 100 times magnification (D-type). The response characteristics of these seismographs are shown in Figure 3. We use the records with unity magnification for the main shock and the largest aftershock at all stations and for the second largest aftershock at HAC, SEN, and NII stations and the records with 100 times magnification for the second largest aftershock at SUT, HAK, OFU, and AIK stations. Since these data were recorded on paper, we first digitized the records, corrected for the instrument response, interpolated at

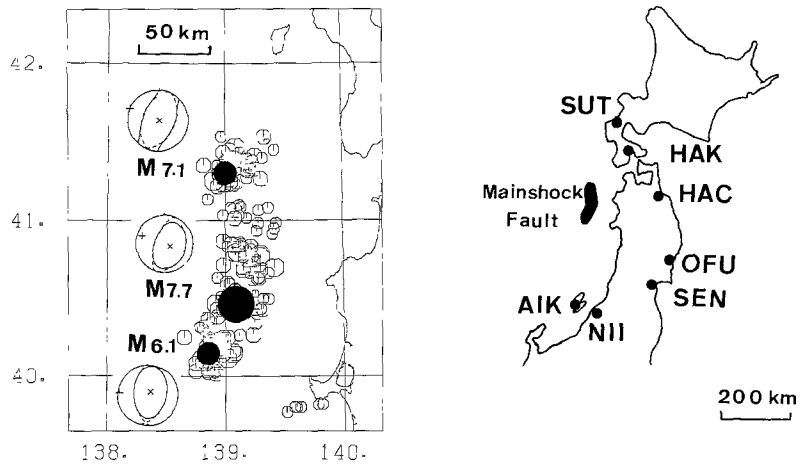

FIG. 2. (*Left*) The locations of the main shock and two largest aftershocks we used in this analysis are shown by the solid circles. Focal mechanisms of these events are shown to the *left* (after Dziewonski *et al.*, 1983) with lower hemisphere, equal-area projection and "+" denotes the pressure axis. (*Right*) The locations of JMA stations we used in this analysis.

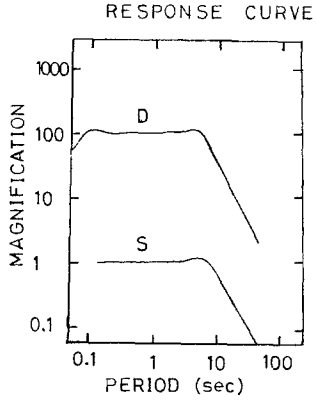

FIG. 3. Characteristic response curves of the JMA strong motion seismometers with magnificatio of 1 and natural period of 6 sec (S-type), and seismometers with magnification of 100 and a natura period of 5 sec (D-type). Both seismometers have the same damping factor ($h = 0.55$).

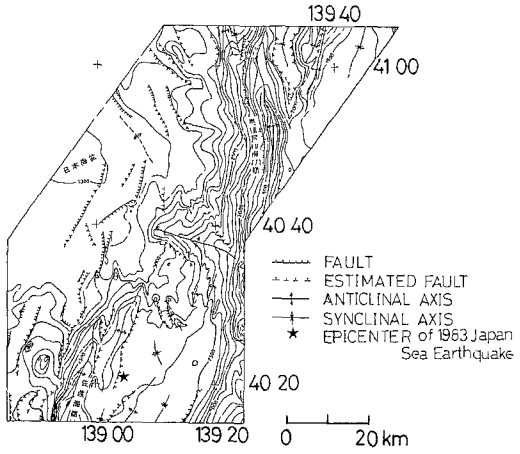

FIG. 4. Geological structure of the main shock region (after Maritime Safety Agency, 1984).

0.1-sec intervals, and then bandpass-filtered from 0.05 to 1.0 Hz. The length of eacl seismic record for the present analysis is 1 min, which contains the major portion with large amplitudes.

FAULT MODEL

Initially, we considered a single fault plane model, and we calculated syntheti seismograms using only one aftershock ($M = 6.1$). This oversimplified mode did not yield an acceptable correspondence between synthetics and observec seismograms.

Next, we used a double fault plane model consisting of two fault surfaces witl different strikes as proposed already by several authors, e.g., Shimazaki and Mor (1983) from surface wave analysis. Geologic mapping (Figure 4) also suggests tha there are two different fault groups with different strike directions in this region As the rupture process would likely be different on each fault surface (Sato, 1983 1985; Ishikawa *et al.*, 1984), we used the aftershock ($M = 7.1$) and the aftershock ($M = 6.1$) for the northern subfault and the southern subfault as empirical Green's functions, respectively. Source parameters and respective fault dimensions adopted here are shown in Table 1. We divided each fault surface into N subfaults (line source case) or $N \times N$ subfaults (area source case), where N is estimated from

equation (2). The seismic moment ratio between the main shock and the corresponding aftershock is estimated by calculating the spectral ratios in the low-frequency range at stations SUT and SEN. The ratios are

$$M_0(M = 7.7)/M_0(M = 6.1) \simeq 300$$

and

$$M_0(M = 7.7)/M_0(M = 7.1) \simeq 10.$$

Following Mori and Shimazaki (1983), we assume that two-thirds of the moment is distributed on the northern fault surface and one third on the southern fault surface. Taking this into account for each subfault, N in equation (2) is calculated as follows

N (southern subfault)

$$= [M_0(\text{southern subfault of mainshock})/M_0(M = 6.1)]^{1/3} = 5 \quad (13)$$

N (northern subfault)

$$= [M_0(\text{northern subfault of mainshock})/M_0(M = 7.1)]^{1/3} = 2. \quad (14)$$

From the above estimates, the main shock fault surface is segmented as shown in Figure 5.

The aftershock area dimensions of the two events used as empirical Green's functions ($M = 6.1$ and $M = 7.1$) are approximately 6×6 and 20×20 km,

TABLE 1

SOURCE PARAMETERS FOR THE FAULT MODEL

	Northern Subfault	Southern Subfault
Length	60 km	30 km
Width	30 km	30 km
Strike	N15°E	N10°W
Dip	20°	20°

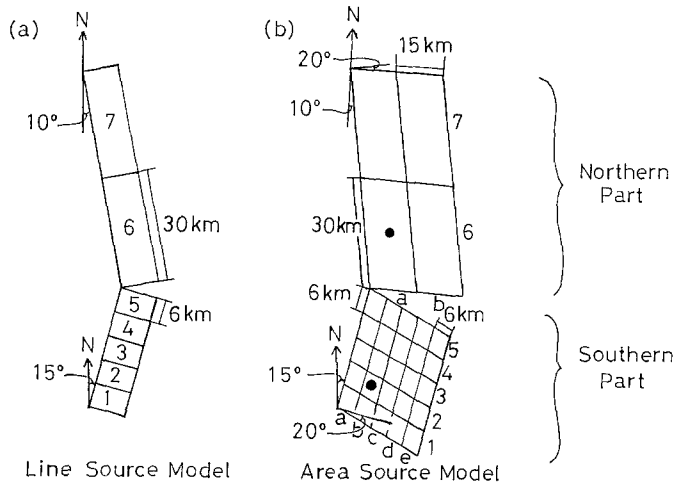

FIG. 5. Fault model assumed in this analysis: (a) line source model and (b) area source model.

respectively (JMA, 1984). These sizes are coincident with the element dimensions we determined from the moment ratio. This suggests the scaling relation on the fault length or width to be approximately held among these three events (M = 7.7 7.1, and 6.1) used in this analysis.

Although parameters m_i and t_i are considered to be model parameters, the rise time at each subfault is assumed to be constant. The observed seismograms have a predominant frequency less than 0.2 Hz. Then, we can assume that the deviation of the rise time has a smaller influence on the main motions compared with the other parameters. In calculating synthetic seismograms, we assume the rise time of the main shock is 4.0 sec so that the rise times of the aftershocks (M = 6.1 and M = 7.1) are estimated to be 0.8 and 2.0 sec, respectively, from equations (1), (2), (13) and (14).

Several authors have reported that the second subevent occurred 23 to 26 sec after the first subevent occurrence (Mori and Shimazaki, 1983; Sato, 1983, 1985 Ishikawa *et al.*, 1984). We adopt 25 sec for the retarded time of the second subevent occurrence when constructing the initial model.

Sato (1983, 1985) showed that the rupture propagated parallel to the fault strike from south to north from the analysis of accelerograms obtained at 10 stations located near the fault region (50 to 200 km). Therefore, we first attempt to apply a finite line source model to estimate the source process as shown in Figure 5a. But at the station perpendicular to the strike direction, the waveforms could not be fully explained using the line source model. Next, we tried to estimate the source process using a finite area source model (Figure 5b).

Results of the Inversion

Line source case. We need a starting model, i.e., a set of initial values to solve the nonlinear inversion problem. We assume that the horizontal component seismograms used in this analysis consist mainly of S wave, and we perform a forward test to get approximate estimates of the parameters. Initially, we assumed that parameters m_i are all unity and t_i are given as the rupture propagated uniformly with the velocity V_r. We varied the rupture velocity V_r to find parameters t_i which makes synthetics agree reasonably well with observations. From the results of the analysis of teleseismic data (Mori and Skimazaki, 1983; Ishikawa *et al.*, 1984) and near-field accelerograms (Sato, 1983, 1985), we assumed that the rupture initiated at element 2, shown in Figure 5a, propagated bilaterally in the southern subfault (elements 1 to 5) and restarted at element 6 in the northern subfault 25 sec after the initial starting time. The attempt to determine the initial values was made by forward modeling, and the resulting synthetic seismograms are shown in Figure 6 This result suggests a rupture velocity of 2.0 km/sec. Thus, we choose parameter t for each subfault consistent with the rupture propagation of 2.0 km/sec as the starting model (Table 2). We assume the covariance matrices E and D defined by (A6) and (A7) are as follows: all off-diagonal elements of both E and D are equal to zero. All diagonal elements of E are equal to 0.3. Diagonal elements of D corresponding to the relative moment releases of northern and southern subfaults and rupture starting times of northern and southern subfaults are equal to 2.0, 1.0, 4.0, and 2.0 respectively.

After approximately ten iteration steps, we obtained a final solution that satisfied the convergence criterion $[(HA)_{tr}/(KI)_{tr} = 0.1]$ of the inversion. The starting model and the final model are shown in Figure 7 and Table 2. Standard deviations for

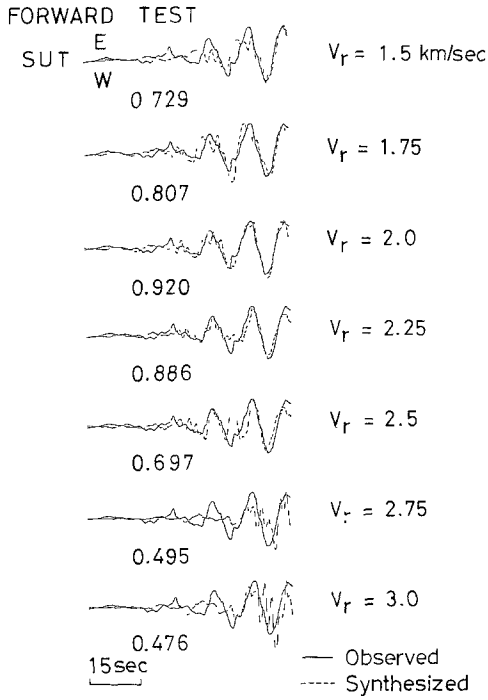

FIG. 6. Forward test for the line source model. Rupture velocity V_r is the only variable. Solid lines are observed seismograms, and dotted lines are synthesized. The numbers plotted below the waves are the values of the cross-correlation.

TABLE 2

RESULTS FOR THE LINE SOURCE MODEL

	Element No						
	1	2	3	4	5	6	7
Starting model							
t_i*	3.0	0.0	3.0	6.0	9.0	25.0	40.0
S.D.†	1.4	1.4	1.4	1.4	1.4	2.0	2.0
m_i*	1.0	1.0	1.0	1.0	1.0	1.0	1.0
S.D.	1.0	1.0	1.0	1.0	1.0	1.4	1.4
Final model							
t_i	2.5	0.5	3.1	5.4	7.4	24.8	40.4
S.D.	0.55	0.39	0.56	0.54	0.50	0.64	0.60
m_i	1.3	1.0	1.0	0.8	0.6	0.7	1.3
S.D.	0.17	0.16	0.14	0.13	0.14	0.09	0.26

* t_i and m_i represent the rupture starting time and relative moment release, respectively.

† S.D. represents the standard deviation.

model parameters are also shown in Table 2. The waveforms which are calculated from the final fault model parameters are shown in Figure 8. The results of the inversion using the line source reveal the heterogeneity of the faulting: (1) the average rupture velocity is approximately 2.0 km/sec for the northern subfault and 2.5 km/sec for the southern subfault, and (2) the relative moment release is highest at the northern edge (element 7) on the northern subfault and at the southern edge (element 1) on the southern subfault. Moreover, it is noted that the rupture

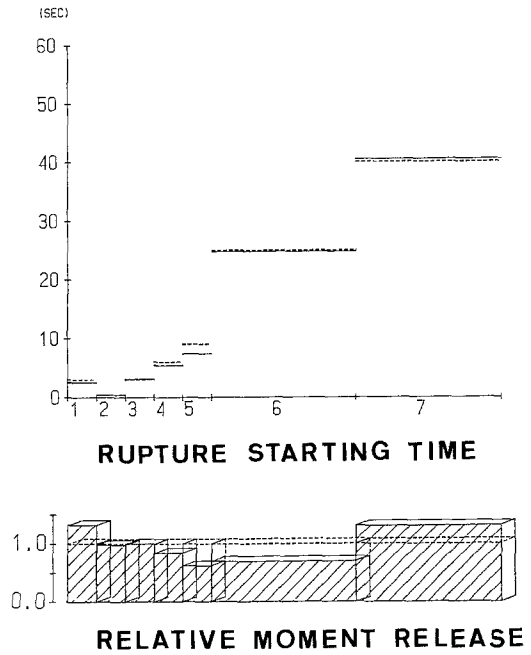

FIG. 7. The results of the inversion for the line source. Dotted lines are the starting model and solid lines are the final model.

propagated smoothly in the southern subfault. These results are assured to be reliable judging from the remarkable decrease of the standard deviations (Table 2).

Area source case. We performed forward modeling for a finite area source model using the same procedure as for the line source to determine the initial model for the inversion. Here again, we fixed parameters m_i to 1 and controlled parameter t_i by varying both the northern subfault rupture velocity and southern subfault rupture velocity. We assumed circular rupture propagation away from an initiation point. From the results of forward modeling, we find the rupture velocities are again approximately 2.0 km/sec along the northern subfault and 2.5 km/sec along the southern subfault, with the rupture initiating at element 2b (Figure 5b), giving similar results as the inversion of the line source case. Then, we use the parameters associated with these rupture velocities to construct the starting model of the inversion (Table 3). We assume the covariance matrices E and D defined by (A6) and (A7) are as follows: all off-diagonal elements of both E and D equal to zero. All diagonal elements of E are equal to 0.3. Diagonal elements of D corresponding to the relative moment releases of northern and southern subfaults and rupture starting times of northern and southern subfaults are equal to 4.0, 2.0, 8.0, and 4.0, respectively.

After approximately five iteration steps, we obtained the final solution, which satisfies the convergence criterion of the inversion $[(HA)_{tr}/(KI)_{tr} = 0.05]$. The parameters of the starting model and final model are shown in Table 3, and the final results are shown in Figure 9. The waveforms which were calculated from the final model are shown in Figure 10. Since standard deviations of the area source parameters are much greater than those for the line source parameters as shown in Table 3, the results obtained here involve some uncertainties. This fact may be partially caused by the increase of the parameter. Since the synthetic seismograms

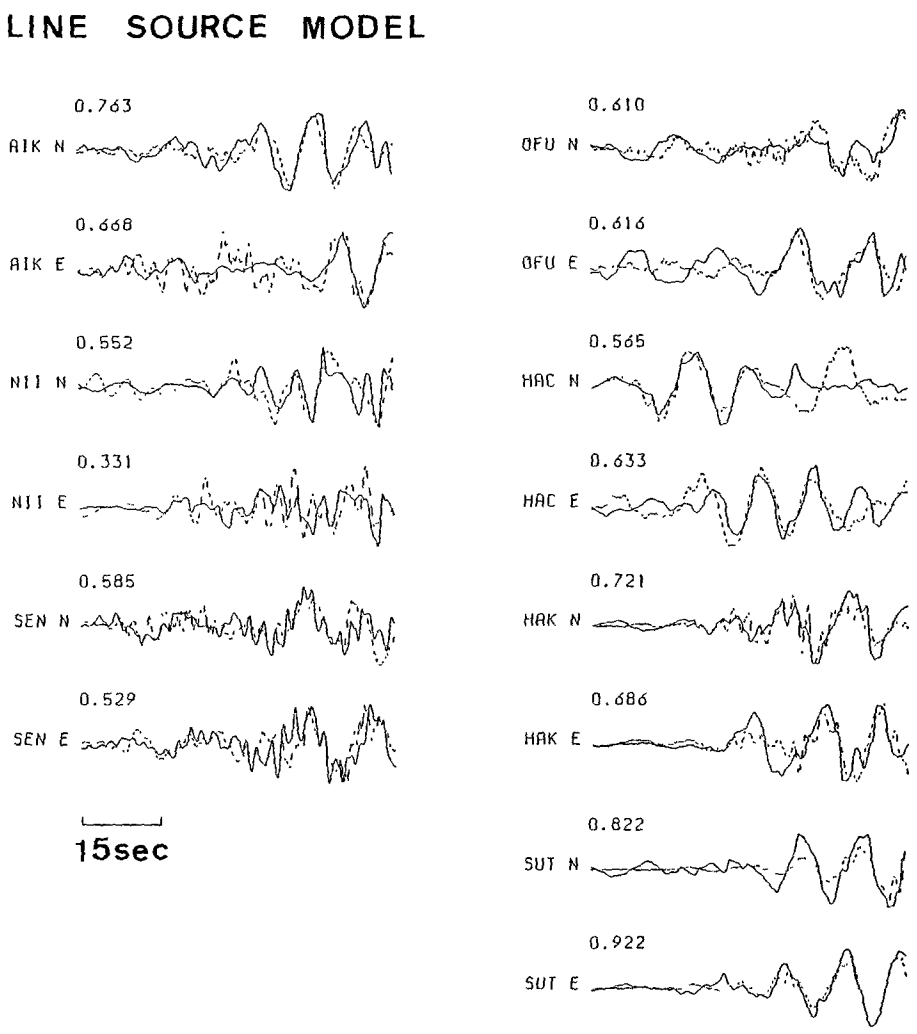

FIG. 8. The waveforms calculated from the final parameters of the line source. Solid lines are observed seismograms and dotted lines are synthesized. The *upper left number* of each trace is the value of the cross-correlation.

for the final model show a better agreement with the observed ones, we consider these results to give the essential characteristics of the two-dimensional source process. The inhomogeneous slip distribution and the nonuniform rupture propagation for the area source model are consistent with those of the line source model.

DISCUSSION

The approach we propose here is a first attempt in applying empirical Green's functions to study fault heterogeneity. There are several aspects that need to be refined in our algorithm, i.e., the waveform synthesis and the inversion procedure.

Empirical Green's functions. We need to evaluate the validity and applicability of the empirical Green's function method. Criteria are needed to determine which event is the most suitable to the empirical Green's function for each element on the fault surface. Here, we used the records from only two large aftershocks, assigning them to the northern subfault and the southern subfault of the main shock surface,

TABLE 3

RESULTS FOR THE AREA SOURCE MODEL

Starting Model										Final Result									
	Southern Subfault						Northern Subfault				Southern Subfault						Northern Subfault		
	Element No	a	b	c	d	e	Element No.	a	b		Element No.	a	b	c	d	e	Element No.	a	b
t_i*		3.4	2.4	3.4	5.4	7.6		25.0	32.5	t_i		2.8	2.3	3.0	5.3	7.4		25.3	32.4
S.D.†		2.0	2.0	2.0	2.0	2.0		2.8	2.8	S.D.		1.84	1.81	1.84	1.86	1.92		1.71	2.57
	1	—	—	—	—	—	6	—	—		1	—	—	—	—	—	6	—	—
m_i*		1.0	1.0	1.0	1.0	1.0		1.0	1.0	m_i		1.4	1.4	1.3	1.2	0.9		0.8	0.1
S.D.		1.4	1.4	1.4	1.4	1.4		2.0	2.0	S.D.		1.38	1.37	1.38	1.39	1.37		0.95	1.00
		2.4	0.0	2.4	4.8	7.2		40.0	41.8			2.3	0.3	2.3	4.7	7.4		41.0	42.7
		2.0	2.0	2.0	2.0	2.0		2.8	2.8			1.80	1.84	1.89	1.93	1.89		1.43	1.64
	2	—	—	—	—	—	7	—	—		2	—	—	—	—	—	7	—	—
		1.0	1.0	1.0	1.0	1.0		1.0	1.0			1.4	1.3	1.1	0.9	0.9		1.3	1.1
		1.4	1.4	1.4	1.4	1.4		2.0	2.0			1.39	1.37	1.38	1.39	1.36		1.55	1.46
		3.4	2.4	3.4	5.4	7.6						3.2	2.0	3.2	5.6	7.9			
		2.0	2.0	2.0	2.0	2.0						1.91	1.89	1.92	1.88	1.87			
	3	—	—	—	—	—					3	—	—	—	—	—			
		1.0	1.0	1.0	1.0	1.0						1.0	1.3	0.9	0.9	1.2			
		1.4	1.4	1.4	1.4	1.4						1.35	1.38	1.38	1.37	1.37			
		5.4	4.8	5.4	6.8	8.7						5.2	5.0	5.6	6.6	8.2			
		2.0	2.0	2.0	2.0	2.0						1.94	1.93	1.90	1.91	1.88			
	4	—	—	—	—	—					4	—	—	—	—	—			
		1.0	1.0	1.0	1.0	1.0						0.5	0.7	0.9	1.1	1.0			
		1.4	1.4	1.4	1.4	1.4						1.34	1.36	1.36	1.38	1.40			
		7.6	7.2	7.6	8.7	10.2						8.0	7.5	7.6	8.5	10.3			
		2.0	2.0	2.0	2.0	2.0						1.93	1.91	1.96	1.97	1.96			
	5	—	—	—	—	—					5	—	—	—	—	—			
		1.0	1.0	1.0	1.0	1.0						0.8	0.6	0.6	0.8	0.6			
		1.4	1.4	1.4	1.4	1.4						1.35	1.37	1.35	1.34	1.36			

* t_i and m_i represent the rupture starting time and relative moment release, respectively.

† S.D. represents the standard deviation.

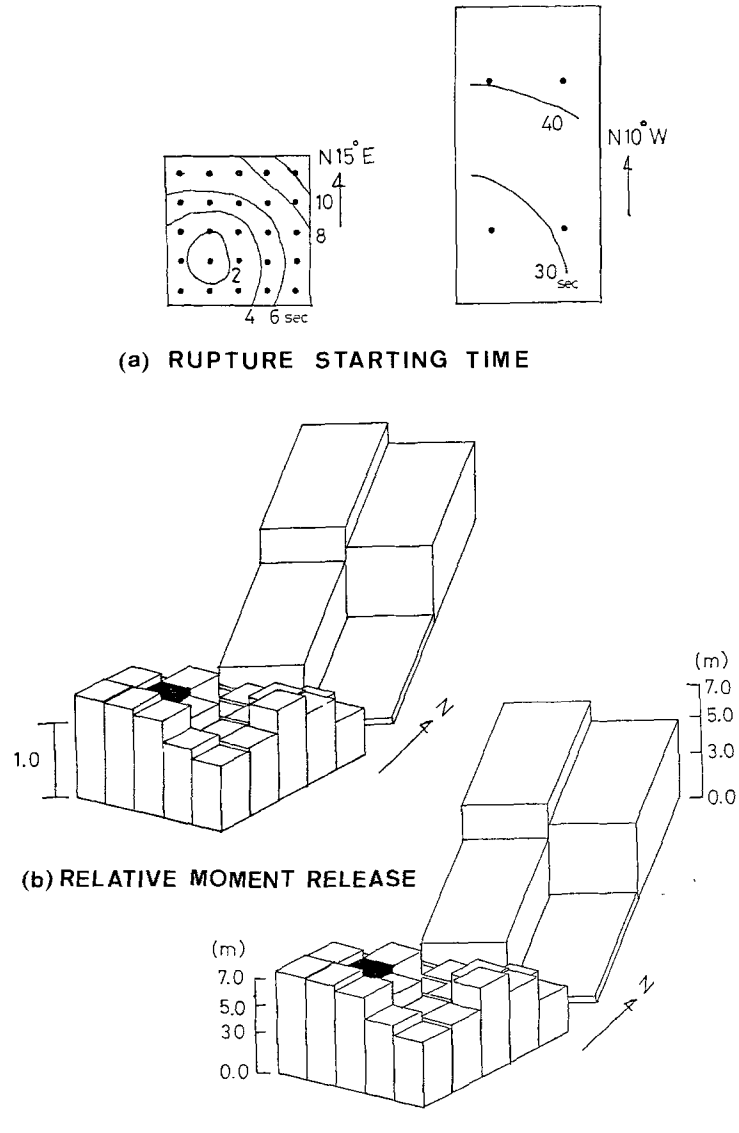

FIG. 9. The results of the inversion for the area source. (a) The rupture starting time on each element. (b) Distribution of the relative moment release. (c) If we assume the total moment equals to 4.55×10^{27} dyne·cm (after Dziewonski *et al.*, 1983) and rigidity equals to 3.5×10^{11} dyne/cm^2, we can translate (b) into the distribution of the slip.

respectively. We used the same records for all elements in each subfault as empirical Green's functions, correcting them only for the time delay that corresponds to the rupture propagation over the fault surface and the seismic propagation from each element to the station, and for the amplitude due to the geometrical spreading factor. This means that we assigned an average Green's function to each element on the fault. The capability to resolve the irregularities on the fault surface is restricted by the size of the available aftershocks. The aftershock of $M = 7.1$, which was used as an empirical Green's function for the northern subfault, may be too large to resolve the fault motion in detail. To improve the resolution of the rupture

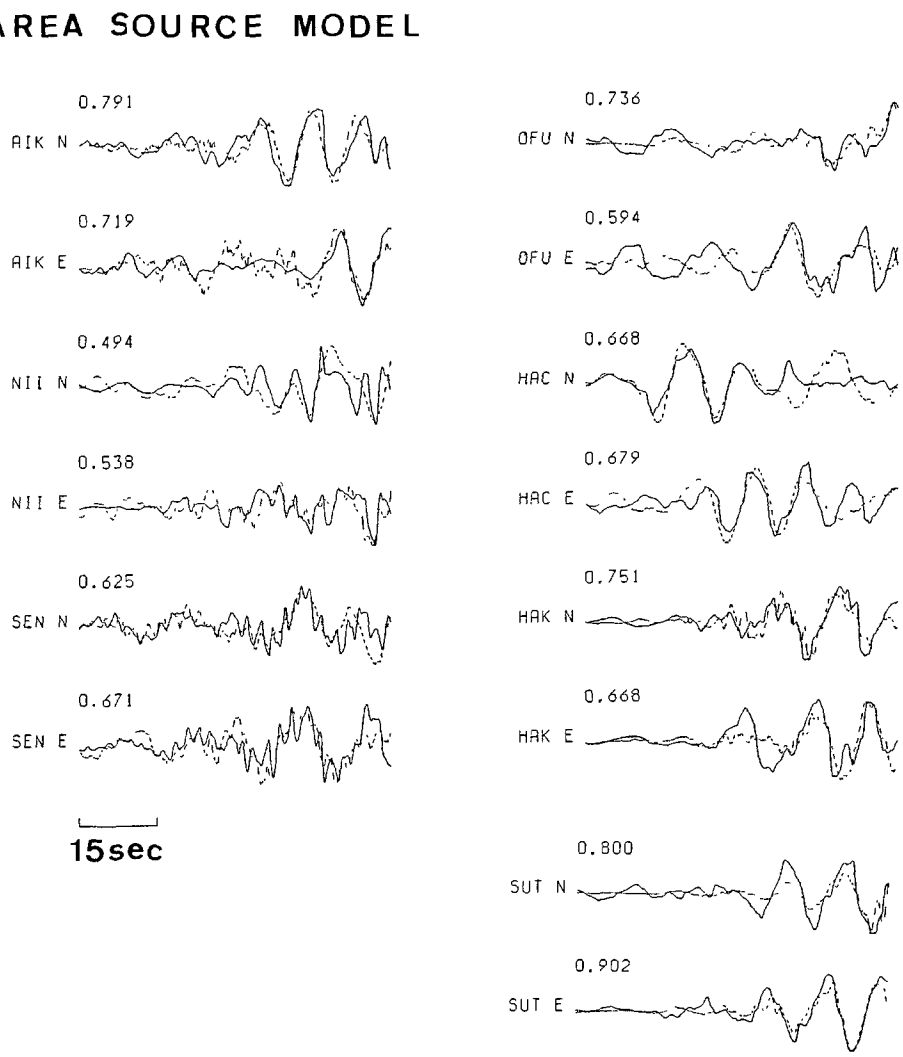

FIG. 10. The waveforms calculated from the final parameters for the area source model.

process, we need to reconstruct the empirical Green's functions using some smaller events that are distributed uniformly within the fault region.

Synthesis method. We can correct for amplitude variation caused by the radiation pattern if we assume the wave type of the records and the focal mechanism. We infer from the travel-time distance curve that the wave motions we treated in this study consist of S waves as well as surface waves locally converted from S waves. We evaluated the influence of radiation pattern on the amplitude variation by calculating the ratio between the radiation pattern of each element and that of the aftershock, assuming that the observed seismograms contain mostly S waves. We found that for almost all of the stations the ratios are within the range of 0.9 and 1.1. Therefore, we can neglect the correction for this effect.

Since the waves of interest are mainly body waves (including surface waves locally converted from body waves) and reflected waves from the reflector inside the earth, p in equation (3), for correcting geometrical spreading factor, might be between 0.5 and 1.0. We calculate the terms (r_e/r_i) and $(r_e/r_i)^{1/2}$ for the worst case of our model,

and we find the difference is within the range of several per cents. This order is as much as or less than that of the estimated errors of the radiation correction term. Therefore, we choose the value of p for the most remarkable phase, i.e., direct body waves.

Total moment. If we exactly know the seismic moments for the aftershocks used as empirical Green's functions, we can calculate the total moment of the main shock using equation (15).

$$M_0^{\text{total}} = m_s(N_s)^3 M_0^{6.1} + m_n(N_n)^3 M_0^{7.1} \tag{15}$$

where m_s and m_n are the means of m_i which belong to the southern and northern subfaults, respectively. N_s and N_n are the numbers determined by equation (2) for the southern and the northern subfaults, respectively. However, in this inversion, we do not estimate the absolute moment of the main shock but only the moment ratio between main shock and its aftershock. According to Dziewonski *et al.* (1983), if we adopt $M_0^{7.1} = 1.9 \times 10^{26}$ dyne·cm and $M_0^{6.1} = 9.6 \times 10^{24}$ dyne·cm, we find the total moment of the main shock to be 3.0×10^{27} dyne·cm. This value is less than that listed in Dziewonski *et al.* (1983) but is comparable to that of Ishikawa *et al.* (1984).

Model parameterization. We evaluate the inhomogeneity of the faulting process by parameter m_i, relative moment release on each subfault. We find that this parameter is very sensitive to the waveform. The variation of parameter m_i corresponds to the variation of the slip velocity. This means physically a variation of the stress drop. The rise time determined by equation (1) is fixed in this analysis because the waveform used in the synthesis has predominant frequencies in the range lower than 0.2 Hz, where the value of the rise time has less influence. Therefore, the variation of parameter m_i may come from variations in the slip displacement distribution.

Data form during inversion. The cross-correlation error function defined by equation (6) and used in this inversion procedure can be expressed after some manipulations

$$y_i = \frac{1}{2} \int [\tilde{O}_i(t) - \tilde{S}_i(t + t_{\max})]^2 \, dt$$

where

$$\tilde{O}_i(t) = O_i(t) \Big/ \left[\int O_i(t)^2 \, dt \right]^{1/2}$$

$$\tilde{S}_i(t) = S_i(t) \Big/ \left[\int S_i(t)^2 \, dt \right]^{1/2}$$

and $O_i(t)$ and $S_i(t)$ are observed and synthesized seismograms of ith station, respectively. This relation shows that minimizing the sum of squares of y_i leads to minimizing the difference between normalized synthetic seismograms and normalized observed seismograms. Therefore, the information on the absolute amplitude as well as the absolute time on each record is automatically removed, and we treat only the waveform information. In our present analysis, it is proper to use the data in the form of cross-correlation error function because it is not so easy to calibrate

the absolute time and absolute amplitude of each seismogram exactly. However, this may be an overreduction of the information contained in the data, especially for the area source model. If we can use high quality data with the absolute time and amplitude, we can extract more information using a different inversion procedure.

Results from the inversion. The bending corner of the fault is a very interesting region. This region, located at the intersection of the Sado ridge and Okushiri ridge (Figure 4), may represent geologically inhomogeneous aspects. Nakamura (1983) suggests the possibility of the existence of a young subduction zone between the North American plate and the Eurasian plate, and this plate boundary crosses this fault at the bending corner. From the results of this analysis (Figures 7 and 9), we find that less moment was released, and rupture propagation was temporarily healed in this region during the main shock. This region may have acted as a geometrical barrier or an inhomogeneous barrier (Aki, 1979) during the main shock.

CONCLUSIONS

The rupture process of the 1983 Japan Sea earthquake has been studied using a nonlinear inversion based on the Bayesian approach by comparing the observed seismograms with synthetic ones derived from empirical Green's functions. The synthetic seismograms and the observed seismograms show a good agreement for almost all of the stations after approximately five iterations. The moment release is maximum at the northern edge and the southern edge of the main shock fault, and minimum around the intermediate region between the southern subfault and the northern subfault of the fault surface. The average rupture velocity is approximately 2.5 km/sec for the southern subfault and 2.0 km/sec for the northern subfault.

ACKNOWLEDGMENTS

The authors wish to thank Professors Soji Yoshikawa, Takeshi Mikumo, Yoshimasa Kobayashi, and Egill Hauksson for constructive reviews of this manuscript. Professors Keiiti Aki and David D. Jackson also gave helpful advice and criticism. Data were provided by Japan Meteorological Agency, and Dr. Shigeru Noda permitted us to use his digitized data of the SENDAI station.

This work was performed while Dr. Irikura was on leave from the Disaster Prevention Research Institute, Kyoto University, as a visiting Professor at the Department of Geological Sciences, University of Southern California. It was partially supported by the National Science Foundation under Grant CEE-8408227.

REFERENCES

Aki, K. (1967). Scaling law of seismic spectrum, *J. Geophys. Res.* **72,** 1217–1231.

Aki, K. (1979). Characterization of barriers on an earthquake fault, *J. Geophys. Res.* **84,** 6140–6148.

Dziewonski, A. M., J. E. Franzen, and J. H. Woodhouse (1983). Centroid-moment tensor solutions for April–June, 1983, *Phys. Earth Planet. Interiors* **33,** 243–249.

Geller, R. J. (1976). Scaling relations for earthquake source parameters and magnitudes, *Bull. Seism. Soc. Am.* **66,** 1501–1523.

Hadley, D. M. and D. V. Helmberger (1980). Simulation of strong ground motions, *Bull. Seism. Soc. Am.* **70,** 617–630.

Hartzell, S. H. (1978). Earthquake aftershocks as Green's functions, *J. Geophys. Res. Letters* **5,** 1–4.

Hartzell, S. H. and T. H. Heaton (1983). Inversion of strong ground motion and teleseismic waveform data for the fault rupture history of the 1979 Imperial Valley, California, earthquake, *Bull. Seism. Soc. Am.* **73,** 1553–1583.

Heaton, T. H. and D. V. Helmberger (1979). Generalized ray models of the San Fernando earthquake, *Bull. Seism. Soc. Am.* **69,** 1311–1341.

Irikura, K. (1983). Semi-empirical estimation of strong ground motions during large earthquakes, *Bull. Disas. Prev Res. Inst., Kyoto Univ.* **33,** 63–104.

Irikura, K. and I. Muramatu (1982). Synthesis of strong ground motions from large earthquakes using observed seismograms of small events, *Proc. 3rd Inter. Earthq. Microzonation Conf., Seattle* **1,** 447–458.

Ishikawa, Y., M. Takeo, N. Hamada, M. Katsumata, K. Satake, K. Abe, M. Kikuchi, K. Sudo, M. Takahashi, S. Kashiwabara, and N. Mikami (1984). Source process of the 1983 Japan Sea earthquake, *Chikyu* **6,** 11–17 (in Japanese).

Jackson, D. D. (1979). The use of *a priori* data to resolve nonuniqueness in linear inversion, *Geophys. J. R. Astr. Soc.* **57,** 137–157.

Jackson, D. D. and M. Matsu'ura (1985). A Bayesian approach to nonlinear inversion, *J. Geophys. Res.* **90,** 581–591.

Japan Meteorological Agency (JMA) (1984). Report on the Nihonkai-Chubu earthquake, 1983, Technical Report of the Japan Meteorological Agency, No. 106 (in Japanese).

Kanamori, H. (1979). A semi-empirical approach to prediction of long-period ground motions from great earthquakes, *Bull. Seism. Soc. Am.* **69,** 1654–1670.

Kanamori, H. and D. L. Anderson (1975). Theoretical basis of some empirical relations in seismology, *Bull. Seism. Soc. Am.* **65,** 1073–1095.

Kikuchi, M. and H. Kanamori (1982). Inversion of complex body wave, *Bull. Seism. Soc. Am.* **72,** 491–506.

Maritime Safety Agency Hydrographic Department (1984). Results of sea bottom survey in 1983 Japan sea earthquake hypocentral region, Report of The Coordinating Committee Earthquake Prediction, Vol. 31, 104–107 (in Japanese).

Mellman, G. R. (1980). A method of body-wave waveform inversion for the determination of earth structure, *Geophys. J. R. Astr. Soc.* **62,** 481–504.

Mori, J. and K. Shimazaki (1983). Source process of the May 26, 1983 Japan sea earthquake, *Abst. Meet. Seism. Soc. Japan* **2,** A16.

Nakamura, K. (1983). Possible nascent trench along the Eastern Japan Sea as the convergent boundary between Eurasian and North American plates, *Bull. Earthquake Res. Inst., Tokyo Univ.* **58,** 711–722 (in Japanese).

Ruff, L. and H. Kanamori (1983). The rupture process and asperity distribution of three great earthquakes from long-period diffracted *P*-waves, *Phys. Earth Planet. Interiors* **31,** 202–230.

Sato, T. (1983). Source properties of the 1983 Japan sea earthquake as inferred from aftershock distribution and strong motion accelerograms, *Ph.D. Thesis,* Tohoku University, Sendai, Japan.

Sato, T. (1985). Rupture characteristics of the 1983 Nihonkai-Chubu (Japan Sea) earthquake as inferred from strong motion accelerograms, *J. Phys. Earth* **33,** 525–557.

Shimazaki, K. and J. Mori (1983). Focal mechanism of the May 26, 1983 Japan sea earthquake, *Abst. Meet. Seism. Soc. Japan* **2,** A15.

Spudich, P. and N. L. Frazer (1984). Use of ray theory to calculate high-frequency radiation from earthquake sources having spatially variable rupture velocity and stress drop, *Bull. Seism. Soc. Am.* **74,** 2061–2082.

Tarantola, A. and B. Valette (1982). Generalized nonlinear inverse problems solved using the least squares criterion, *Rev. Geophys. Space Phys.* **20,** 219–232.

DISASTER PREVENTION RESEARCH INSTITUTE
KYOTO UNIVERSITY
UJI, KYOTO 611, JAPAN

Manuscript received 19 February 1986

APPENDIX

We consider the inversion problem that data vector y can be expressed by the model parameter vecotr x and random error vector $\boldsymbol{e}$ with the form

$$y = f(x^*) + \boldsymbol{e} \tag{A1}$$

where f is the model function and superscript * denotes the true value. We solve (A1) using the Bayesian approach, which was proposed by Jackson and Matsu'ura (1985). The Bayesian approach has an advantage that *a priori* information, which

was found by other analysis, can be directly incorporated. *A priori* information is expressed in the form of initial estimates of the parameters, x_0 and the relation

$$x_0 = x^* + \boldsymbol{d} \tag{A2}$$

where $\boldsymbol{d}$ is an unknown error vector of *a priori* estimates. We incorporate *a priori* information by Bayesian rule

$$P(x \mid y) = P(y \mid x) \cdot P(x)/P(y) \tag{A3}$$

Here, $P(x \mid y)$ is *a posteriori* joint probability density function for the parameters, $P(y \mid x)$ is equivalent to $P(e)$, $P(x)$ is *a priori* joint probability density function of the parameters, and $P(y)$ is a normalizing factor.

For the hypothetical solution x, we define the residuals of observational and *a priori* data as

$$e = y - f(x) \tag{A4}$$

$$d = x_0 - x. \tag{A5}$$

Suppose these errors are Gaussian with zero means and covariance matrix E and D, respectively, i.e.,

$$e \sim N(0, E) \tag{A6}$$

$$d \sim N(0, D). \tag{A7}$$

Then, *a posteriori* probability density function is

$$P(x \mid y) = a \exp(-T^2/2) \tag{A8}$$

where

$$T^2 = e^T E^{-1} e + d^T D^{-1} d. \tag{A9}$$

We can obtain the maximum likelihood solution by minimizing (A9). The solution can be found by solving the implicit equation

$$A^T E^{-1} e + D^{-1} d = 0 \tag{A10}$$

where

$$A_{ij} = (\partial f_i / \partial x_j)_x. \tag{A11}$$